DESY Sumer Student Program 2010

# Analysis of Spray Deposition Technique

**Jessica Lucénius and Andrew Akbashev**

Supervisors

Dr. Stephan V. Roth
Matthias Schwartzkopf
Dr. Jan Perlich

20th July -9th September

# Table of contents

# Analysis of simple Spray Deposition Technique

## Introduction

The search for new and efficient routes for the deposition of films and coatings has always been on the frontier of science owing to its tremendous demand in technology and industry. Today a great variety of deposition techniques is known, but still most of them require special procedures or conditions like vacuum and high temperature (CVD [1, 2], MBE [3], PVD [4]), special chemical environment (Liquid Phase Deposition [5]), varying electrochemical potential (Electrochemical Deposition [6]), a continuing spinning of a substrate (Spin Coating [7]), post-deposition annealing. Although each deposition technique is made to fulfill its own task, it is always a few of them that have been integrated into modern industry. Conventional Spray Deposition (SD) is unique in sense of its simplicity, flexibility and relatively low price.[8] It is widely used for producing polyelectrolyte films [9], multilayered polymer structures for optoelectronic applications [10], semiconductor thin films [11], polymer-based nanocomposite dielectric films [12] or organic bulk heterojunction solar cells [13, 14].

## Experimental section of spraying

As a spray deposition device we used an airbrush "EVOLUTION solo" by Harder&Steenbeck Co. with a nozzle diameter of 0.2 mm and an applied inner gas (Ar) pressure of 1.5-4.5 bar. The distance between the nozzle and a target was varied from 1 cm to 15 cm with 0.1-1 s deposition time. Two ink solutions in ethanol (E-I) and water (W-I) were sprayed on a hydrophobic plastic surface. The diameters of resulting spots were measured using a micrometer. Since such spots tend to be drying very fast, their diameters were marked right after deposition. The deposition conditions such as temperature and humidity were kept constant (21-22 °C and 50-60%, respectively).

Some samples were additionally obtained by Langmuir-Blodgett (LB) technique in order to investigate the difference in film morphologies and structures made by SD and LB. This sophisticated method is often used to controllably prepare thin films. In our Langmuir-Blodgett experiments the amphiphilic molecules were first distributed over the water surface, then the reduction of the area lead to dense packing of surfactant molecules in 2D. While the substrate was moved from under the water through the molecules on a surface, a monolayer of amphiphilic molecules was slowly depositing on a substrate.

## Lanqmuir-Blodgett experiments

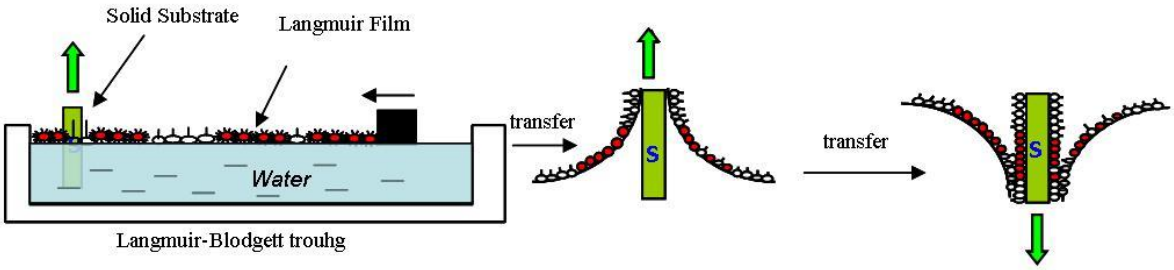


*Scheme 1. Languir-Blodgett method [26]*

Langmuir-Blodgett was also used to prepare samples. In Langmuir-Blodgett method amphiphilic molecules are first deposited on the surface. When reducing the area the surface pressure increases and a phase transition from gas to liquid occur. Surfactant molecules pack very closely in to a solid state, the forming monolayer reduces the surface tension. A schematic layout of the Langmuir-Blodgett method is shown in scheme 1.

# Results

Most E-I spots contained two distinguishable regions: the inner circular part (inner spot) and "arm"-like outer surroundings (outer spot or rim). Depending on the deposition time and the gas pressure in the spray device, the size of the observed "arms" changed. At very short distances (~ 1-2 cm) the inner and outer spot sizes grew if the pressure became higher. Expectedly, the spot size decreased with shorter pulse time.

For short pulses the "arms" were observed up to 2 cm distance for 1.5 bar pressure, to 3.5 cm for 3 bar and to 4.5 cm for 4.5 bar, their sizes gradually becoming smaller with increasing distance. At some point no inner or outer parts can be distinguished. This corresponding distance we call the transition distance. At larger distances the spot structure could also be differentiated into two regions with certainly different ink contrast. The usual inner region had intense contrast and contained relatively large droplets (~ 500 µm) whilst the outer spot contrast became more faded at larger distance away from the spot center. Noteworthy, no transition onset was found in case of deposition at 4.5 bar and 1 s pulse time.
The spots made with W-I solution revealed different structure. Instead of "arms"-like outer and inner homogeneous regions, the W-I-made spots have two clearly distinguishable regions at short deposition distance (1 – 5 cm) – outer with large droplets (~1-2 mm) and inner with small droplets (~ 200-500 µm). Since the resulting spots looked completely different from the E-I-made spots, we cannot directly compare these two types of samples. As a certain difference from what was observed earlier, a broad heap is found to take place at pressure of 1.5 and 3 bar. Once the deposition was made under the pressure of 4.5 bar, the outer spot diameter did not become shorter with increasing distance as in other cases, but was enlarging to

relatively high value. Also no apparent change in size was observed for inner spot diameter. It is worth pointing out that an indirect transition point took place for all series of W-I-based samples at ~ 5-6 cm. We call it “indirect” because of its different appearance. Although at short distances (less than 5 cm) the inner region was formed by very small droplets and the outer region by big droplets, at large deposition distances (more than 6) it turned out to be vice versa, thus such samples exhibited a higher droplet growth rate in the center of the spot rather than in the outer region.

In figures 1-9 the results are shown. The red curve for W-I samples in figure 9 shows the dependence of the mist region (not the discussed above outer region) on the distance to the spray nozzle.

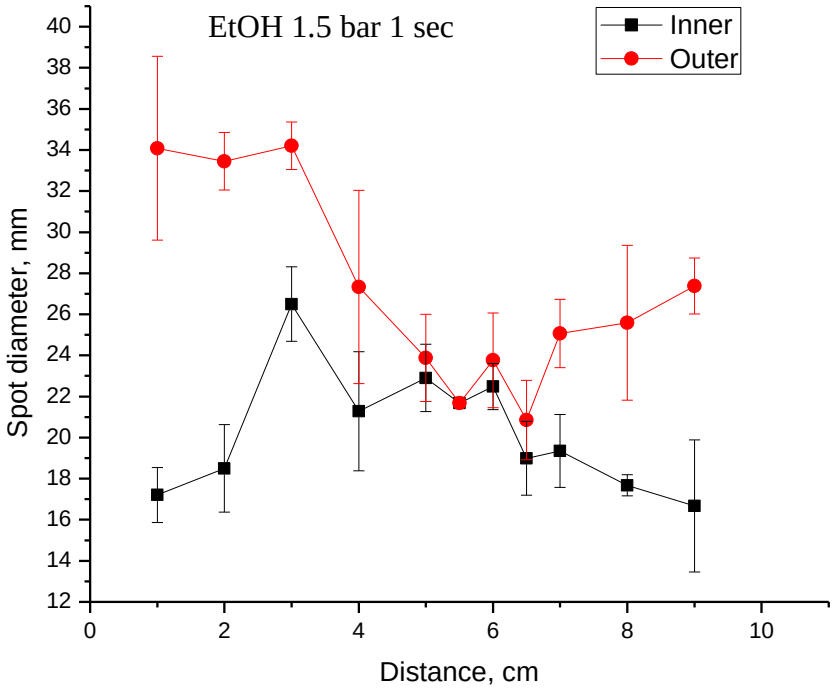


Figure. 1. The outer and inner spot diameters for E-I solution sprayed at 1.5 bar and with 1 s pulse.

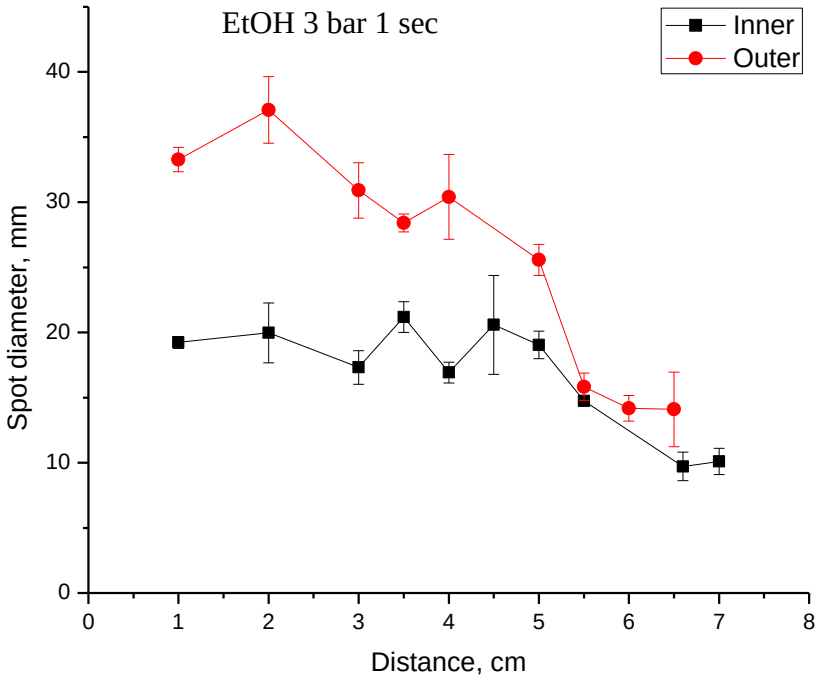


*Fiqure.2 Outer and inner spot diameters for E-I solution sprayed at 3.0 bar with 1s pulse.*

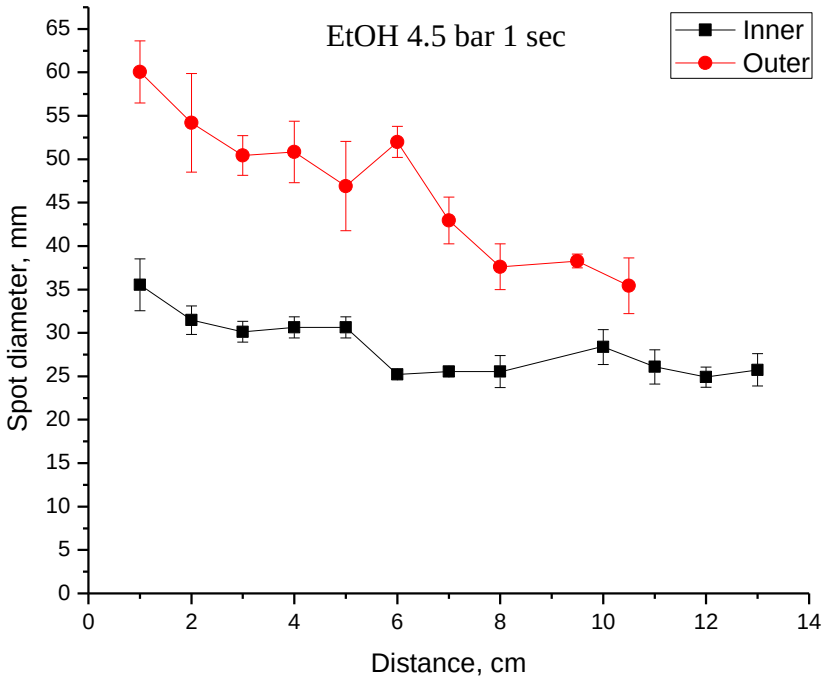


Figure. 3. The outer and inner spot diameters for E-I solution sprayed at 4.5 bar and with 1 s pulse.

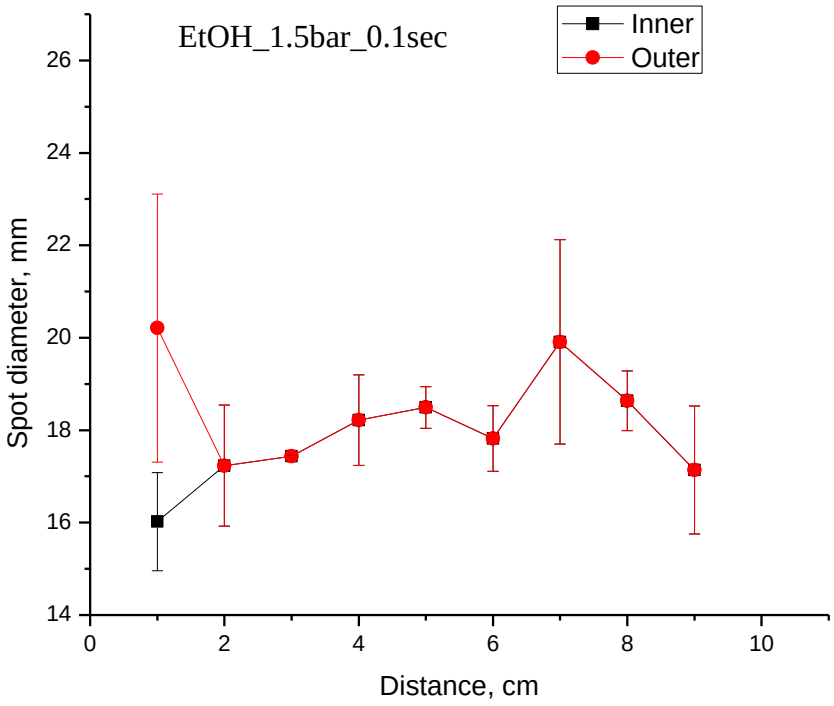


Figure. 4. The outer and inner spot diameters for E-I solution sprayed at 1.5 bar and with 0.1 s pulse.

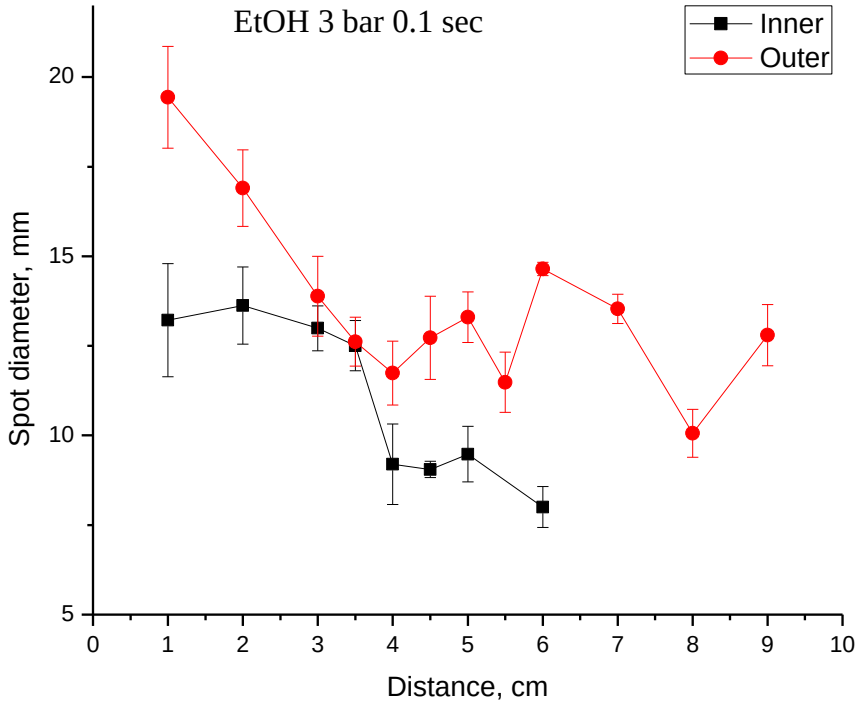


Figure. 5. The outer and inner spot diameters for E-I solution sprayed at 3 bar and with 0.1 s pulse.

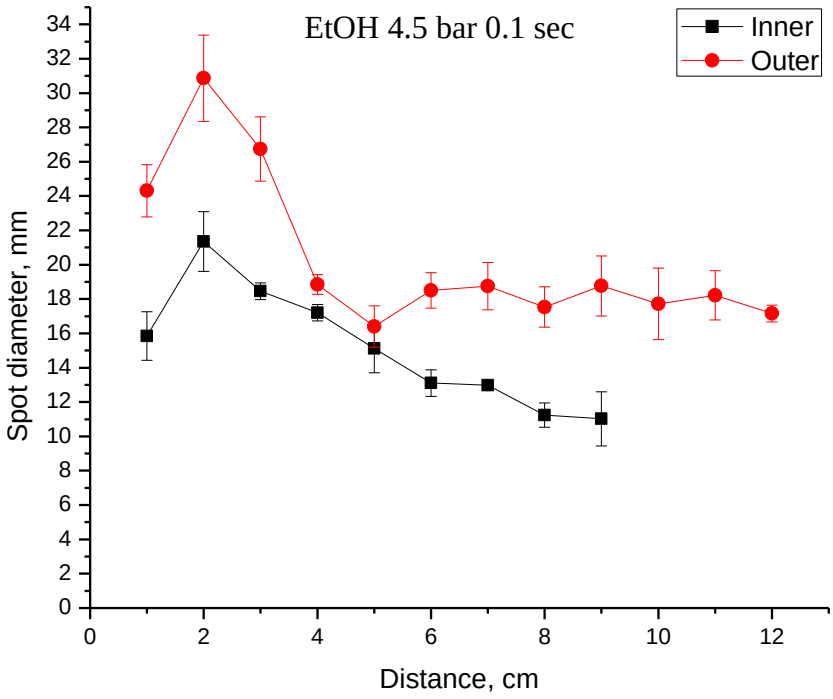


Figure. 6. The outer and inner spot diameters for E-I solution sprayed at 4.5 bar and with 0.1 s pulse.

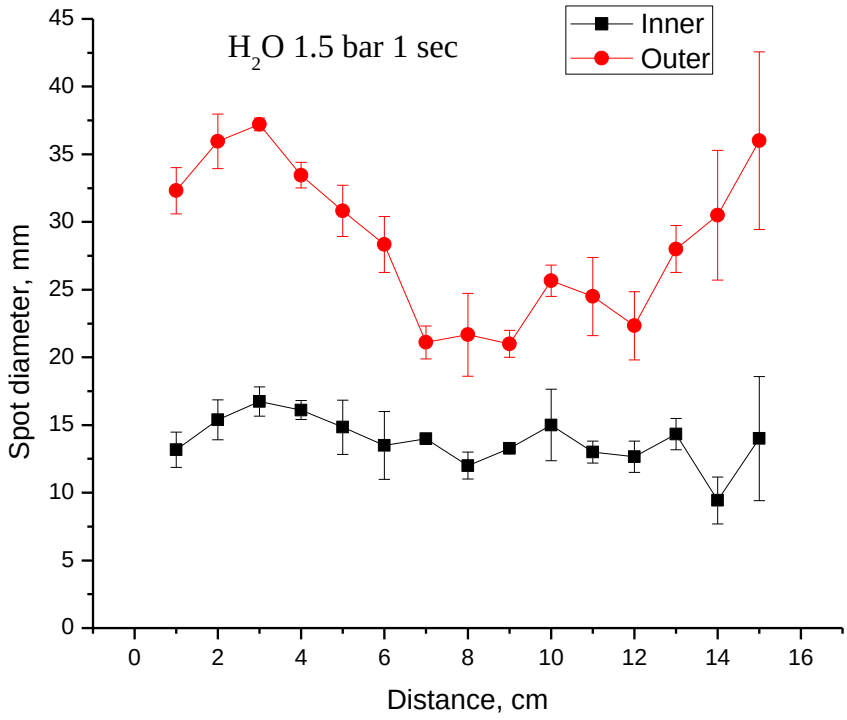


Figure. 7. The outer and inner spot diameters for W-I solution made at 1.5 bar and with 1 s pulse.

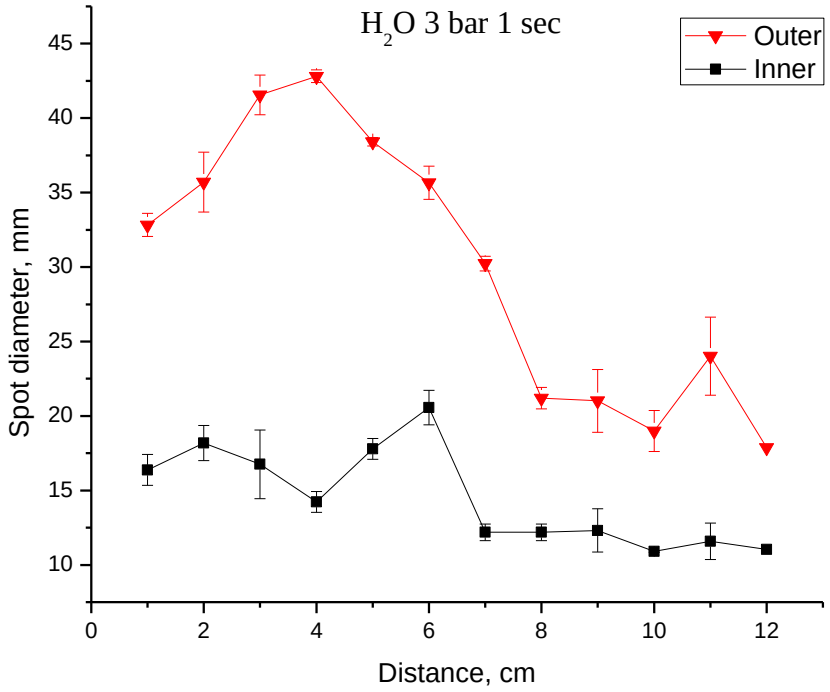


Figure. 8. The outer and inner spot diameters for W-I solution sprayed at 3 bar and with 1 s pulse.

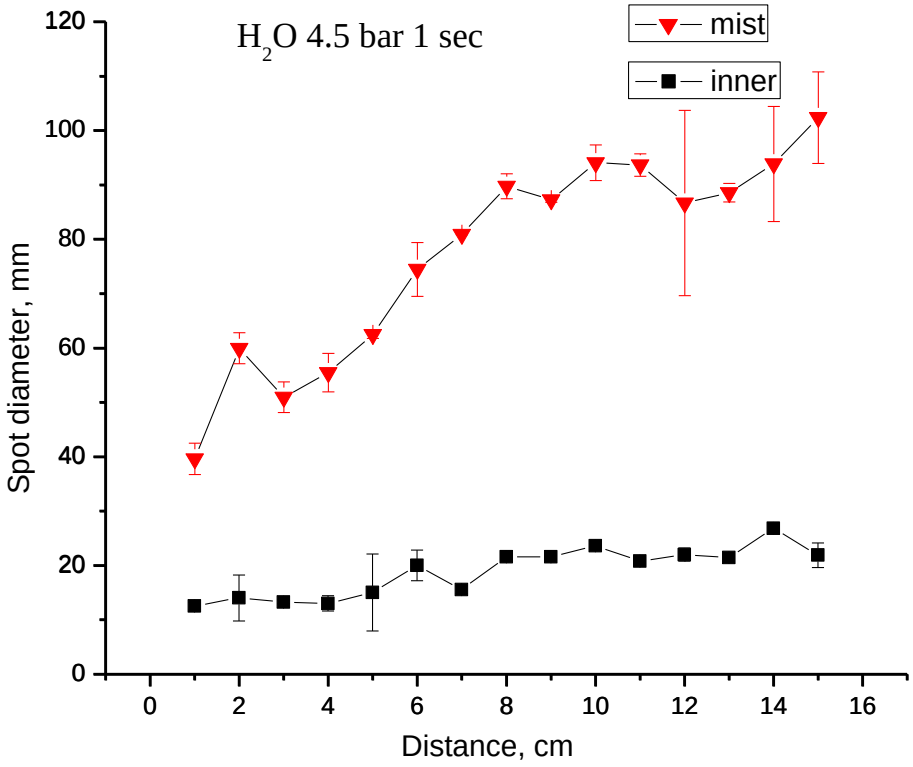


Figure. 9. The outer and inner spot diameters for W-I solution sprayed at 4.5 bar and with 1 s pulse.

# Discussion

To understand the origin of the observed spot structure let us consider a simple model of spray deposition [15]. In figure 10 a scheme of the droplet track distribution in the spray cone and the observed corresponding spot structures are depicted both for EtOH and water. Basically, one may distinguish four different regions along the spray stream. The first is a laminar flow where the motion is uniform which usually corresponds to 3-7 diameters of a nozzle. Then the jet becomes more unstable showing its tendency to expand and thus making random turbulent subflows. At larger distances from the nozzle the amount of subflows consequently grows producing a fully turbulent flow. In the end the flow becomes a mist-like stream which deposition takes place at relatively slow velocity of the solution droplets. All distances associated with the described jet structures strongly depend on pressure, temperature and the viscosity of solution.

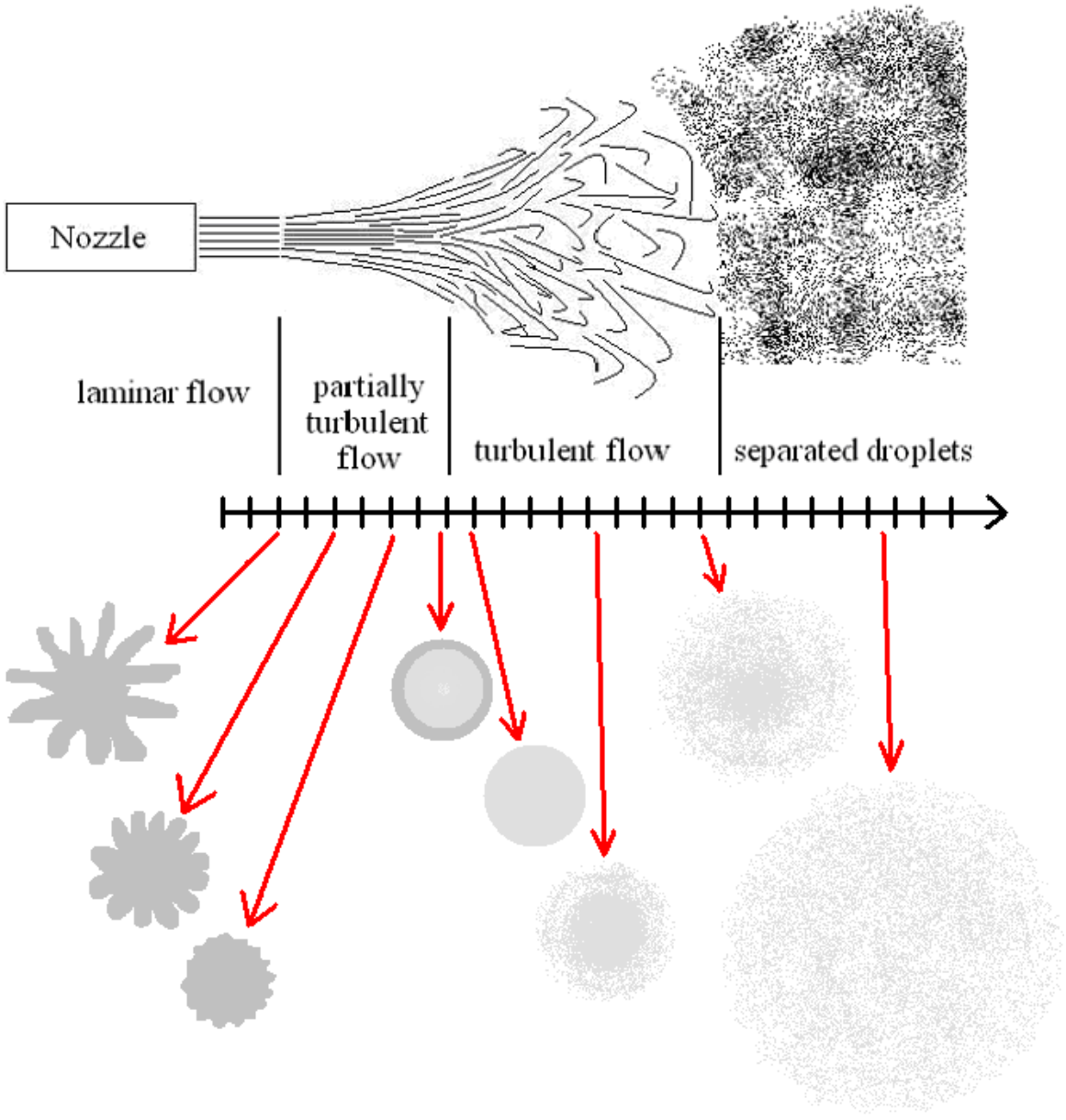


Figure. 10(a). Velocity distribution in a spray cone and the corresponding spot structure for EtOH solution.

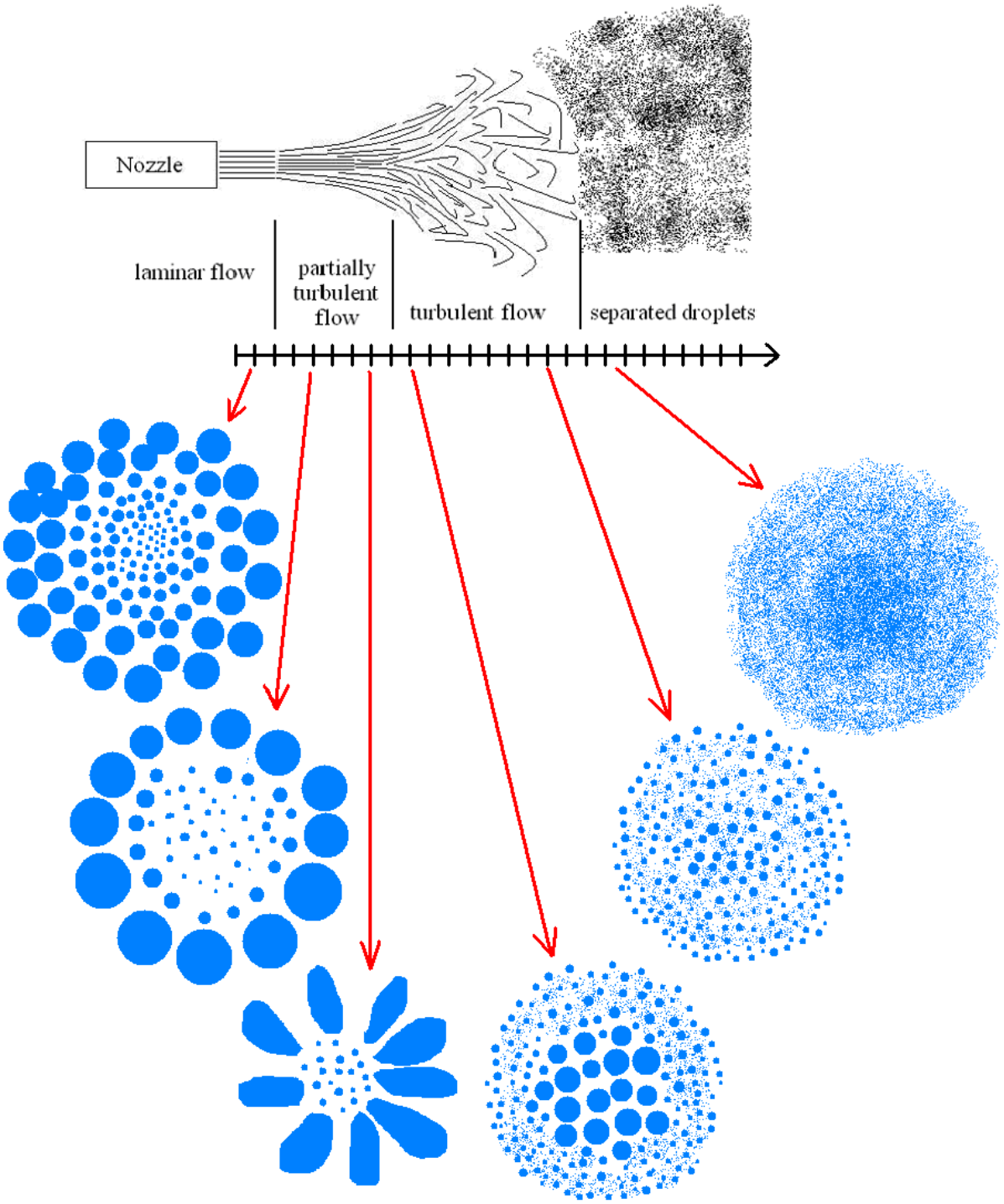


Figure. 10(b). Velocity distribution in a spray cone and the corresponding spot structure for EtOH solution.

In figure 1-3 an expectable and gradual shift of the transition distance to larger values is seen with increasing pressure in the nozzle. Once the gas pressure is increased, the two imaginable boarders where (1) partial turbulence turns into fully turbulent flow and (2) strongly turbulent flow is still present are shifting away from the nozzle, thus moving away the transition distance. One also might notice the general tendency for the curves to shift up that proves the explanation described above. At higher pressure the gas-solution flow affects the target surface much stronger. Consequently, the outer fluid ring that forms under the flow pressure spreads out more than in case of a lower pressure. On the other hand, the surface tension holds

the liquid not allowing it to stream in different directions (figure 11). Thus, if the flow pressure is high enough, it forces the liquid ring to break and numerous streams appear looking as “arms”-like structures coming away from the spot center. Therefore, the higher the pressure in the nozzle is, the larger the inner and outer spot sizes become.

At the transition point the surface tension is equal to the flow pressure, hence the spot is not a double-region, but more or less homogeneous with a little less contrast in the center. At this point the liquid is usually distributed without voids which make us propose this transition distance as the optimum for the deposition of *continuous and smooth films*. At larger distances a different scenario takes place (figure 12). Under a low flow pressure the substrate is covered by small droplets with a homogeneous spot in the center, although the achieved homogeneity strictly depends on the pulse time. In case of lower pulse times, as will be shown below, the spot cannot be considered as a continuous film without voids. Higher pressure shifts the cone structure to larger distances, thus producing a better-quality spot compared to low-pressure deposition. Hence, one can imagine that the increase in pressure makes similar effect on the spot structure as the shift of the target closer to the spray source.

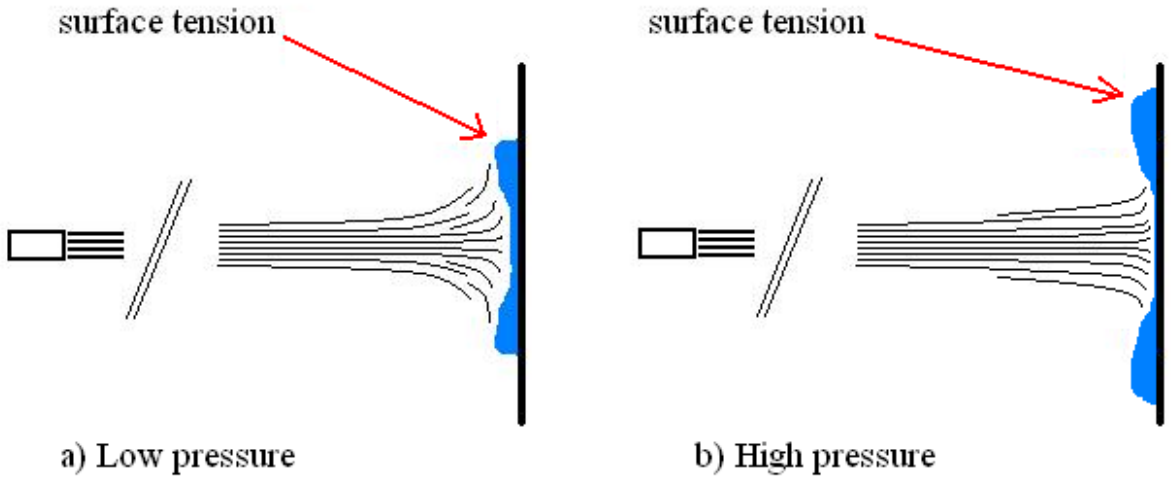


Figure 11. The opposition of the surface tension and the flow pressure.

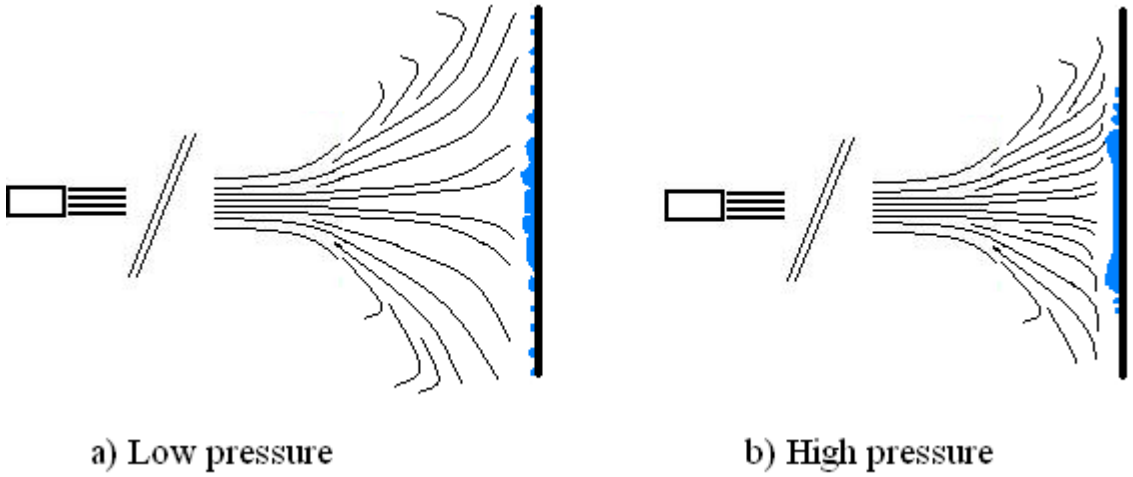


Figure 12. The formation of the spot at large distances from the nozzle.

There are two discrepancies between the discussed long spray pulses (~ 1s) and the short pulses (~10 times shorter). The reason for this discrepancies is the amount of liquid that reaches the substrate and the time during which the sample is exposed to continuous gas flow. The results for the sample obtained with an applied gas pressure of 1.5 bar suggest that the onset of the transition occurs at a very close distance (~ 2 cm). After this point the spot structure corresponds to the case depicted in figure 12(a, b). From fgure 4-6 it is clearly seen that the transition point shifts to larger distance if the pressure in the nozzle increases. It can be explained as the result of an application of a higher spray pressure to the substrate and a larger liquid volume deposited on the surface.

The W-I samples show a completely different behavior. The absence of the "arms"-like structure is connected with a high hydrophobicity of the sample surface. The deposited liquid droplets tend to coalesce into big drops (~1-3 mm) that were subsequently moved away from the center by the in-plane flow. They cannot be considered as "arms" observed in E-I spots since the "arms" were streams from the perfectly round spots, and in W-I case they were single drops that did not made traces as the surface was hydrophobic. At some distance the indirect transition was noted to exist. It has the same origin as for the E-I samples and is explained in terms of the competing surface tension and the in-plane flow pressure. At short distance the flow pressure is high enough to win against the surface tension and to move drops on the substrate which results in the absence of big drops in the center. Once the flow pressure becomes equal to the surface tension, the drops do not move any more and the outer region is only made by small droplets (mist). Further increase in distance makes the liquid-gas stream so thin that the coalescence of droplets on the surface slowly becomes negligible, leaving the inner and outer spot regions almost indistinguishable. Right after deposition the mist region is seen, appearing as the imprint of the cone cross-section at a certain distance. The mist region was characterized by optical microscopy that revealed its island-like morphology without any continuous film formed. One might try to achieve certain continuality during a longer deposition.

The flow rate measurements are presented below. A strong deviation from the linear behavior at high pressure of 4.5 bar can be attributed to the gas flow instabilities inside the nozzle that causes less fluid to join the flow. In other words, the flow at high internal gas pressure consists of almost twice as less liquid as at lower pressure (3 bar).

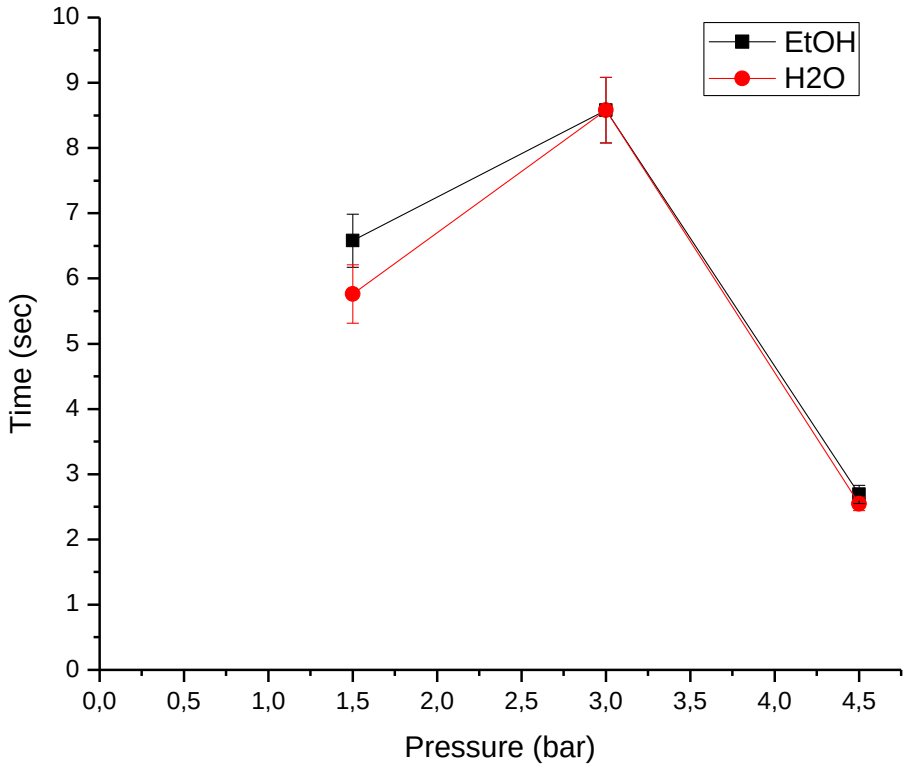


Figure 13. Flow rate measurements

Furthermore, samples with polystyrene spheres (PSS) (diameter ~ 100 nm) deposited by SD technique on a $SiO_2$/Si substrate from ethanol and water solutions with different concentrations were prepared. The deposition conditions were chosen based on the results of the ink solution deposition described above. Thus, pressure equal to 1.5 bar and 3 bar was used. Since at the transition distance samples obtained from ink solution showed the best homogeneity, the distance for PSS deposition was chosen to be 4 and 8 cm.

## Optical microscopy

Optical microscopy (OM) images of the prepared samples are discussed below.

Depending on deposition conditions the spot centre can be easily distinguished (figure 14) from the outer part compared to the indistinguishable case (figure 15).

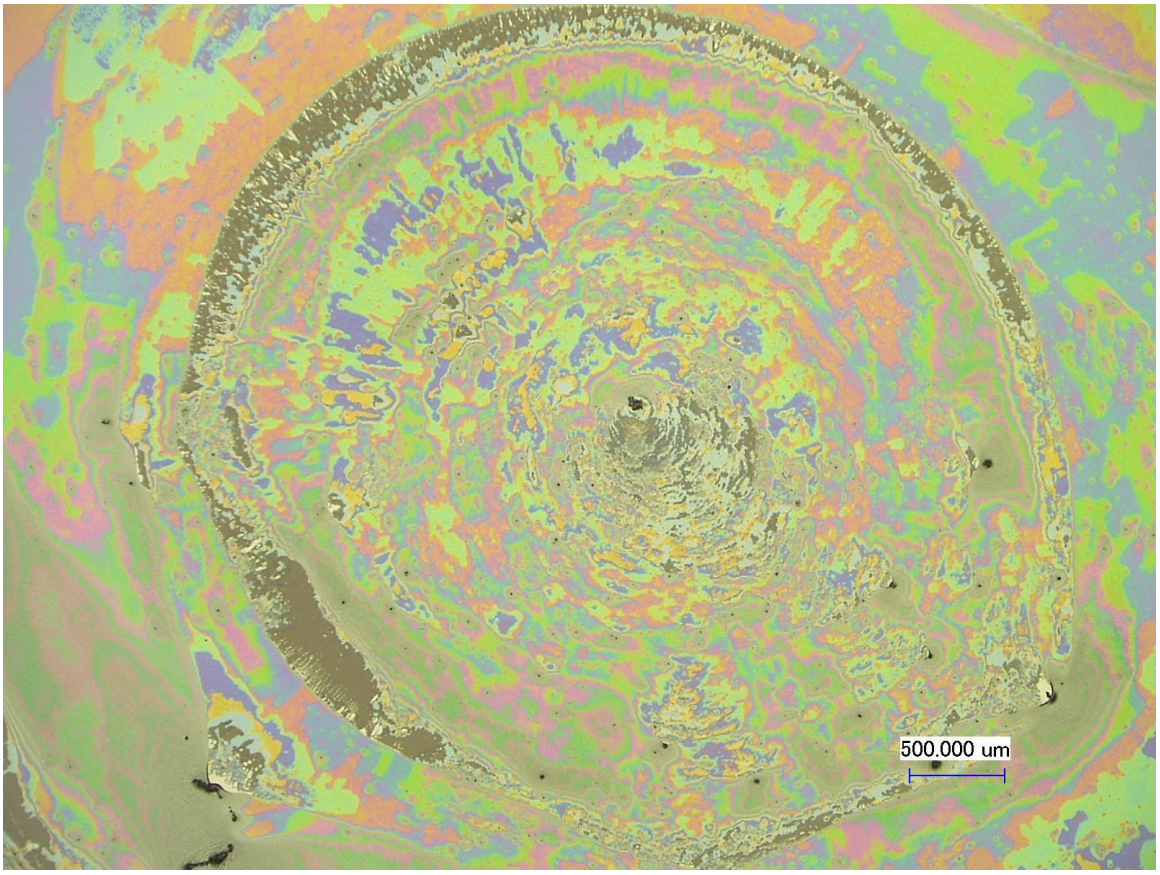

Figure 14. Spot centre for PSS-$H_2O$ solution (6.25 mg/ml) made during 1 s at 3 bar (8 cm).

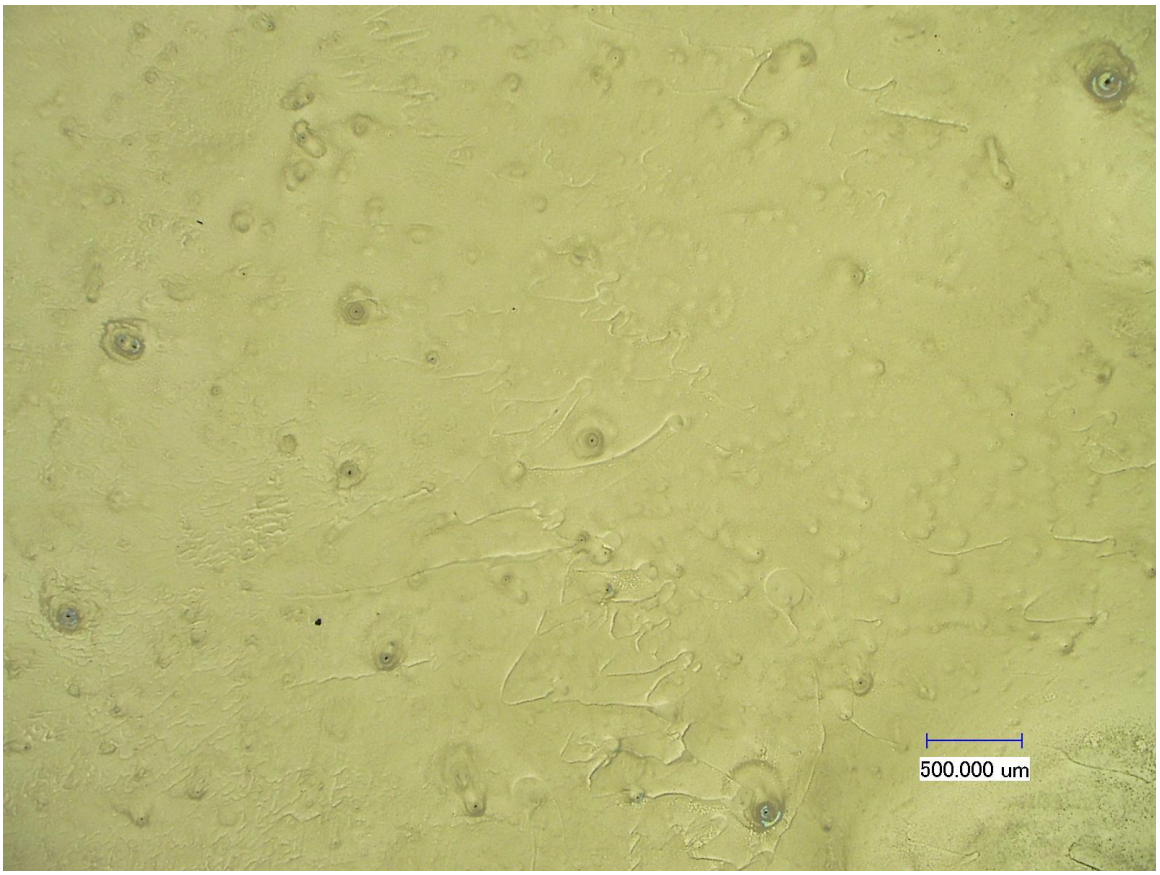

Figure 15. Spot centre for PSS-EtOH solution (6.25 mg/ml) made during 0.2 s at 1.5 bar (8 cm).

For EtOH-based solution the spot centre usually consisted of light-brown region with dark-brown inclusions. The more concentrated the solution, the more density of inclusions is observed on a surface (compare figure 16 and 17). Since the diameter of a PSS sphere is approx. 100 nm, on average a brown colour is expected to be seen due to Fabry–Pérot interference of a visible light, thus we believe these dark small regions are most likely PSS monolayer islands on a substrate.

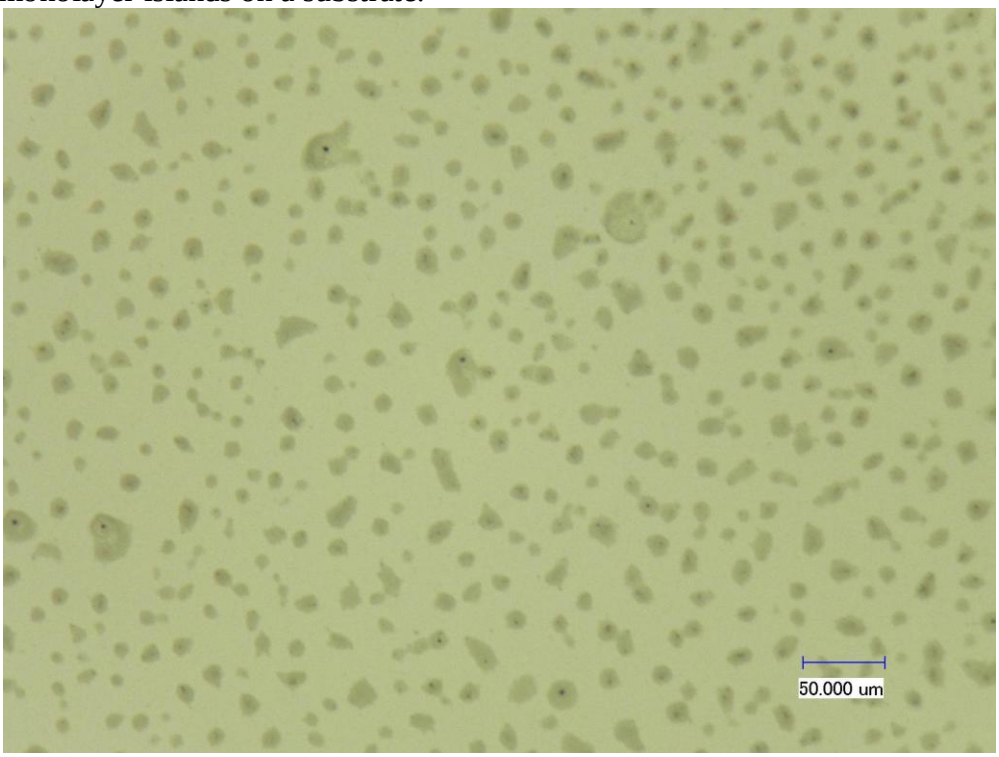


Figure 16. Spot centre for PSS-EtOH solution (0.75 mg/ml, 0.2 s at 1.5 bar, 8 cm).

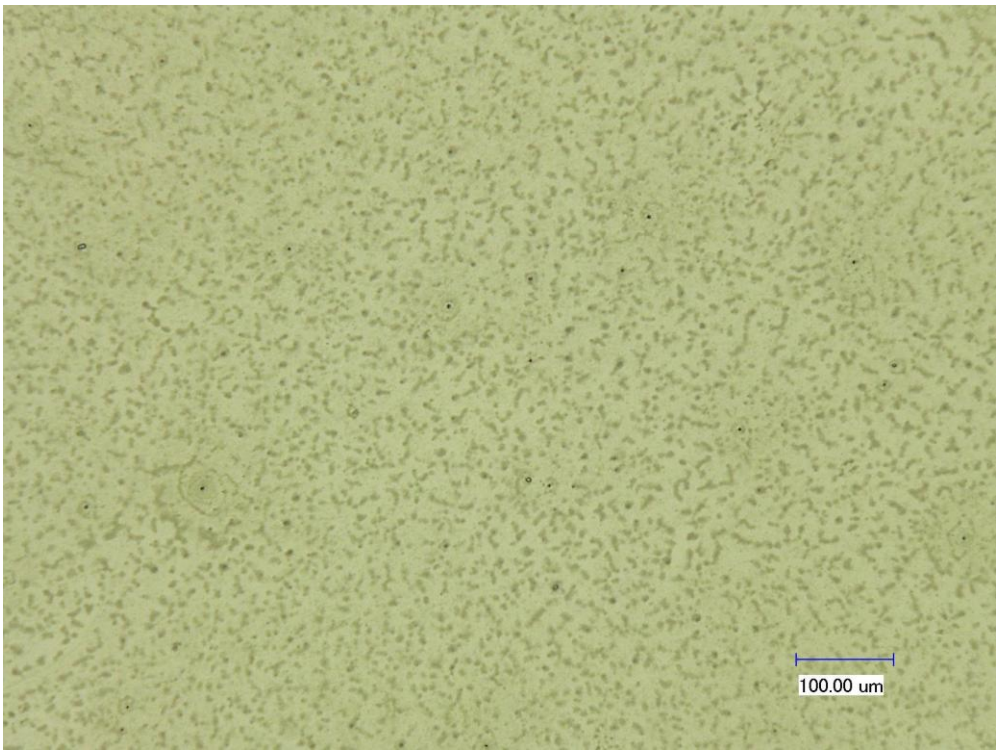


Figure 17. S  spot centre for PSS-EtOH solution (1.56 mg/ml, 0.2 s at 1.5 bar, 8 cm).

It has to be pointed out that a ring made of different colours was observed on the edge of many spots (figure 18). If the concentration in the solution became higher, the space that colour regions took was increasing. Such areas have colour owing to the multilayer PSS film formed after drying. Thus, it is better to use low-concentration solution (< 1.56 mg/ml) for the deposition of a monolayer film. A highly probable formation of colour regions is also noted to occur if the turbulence took place on a surface during deposition.

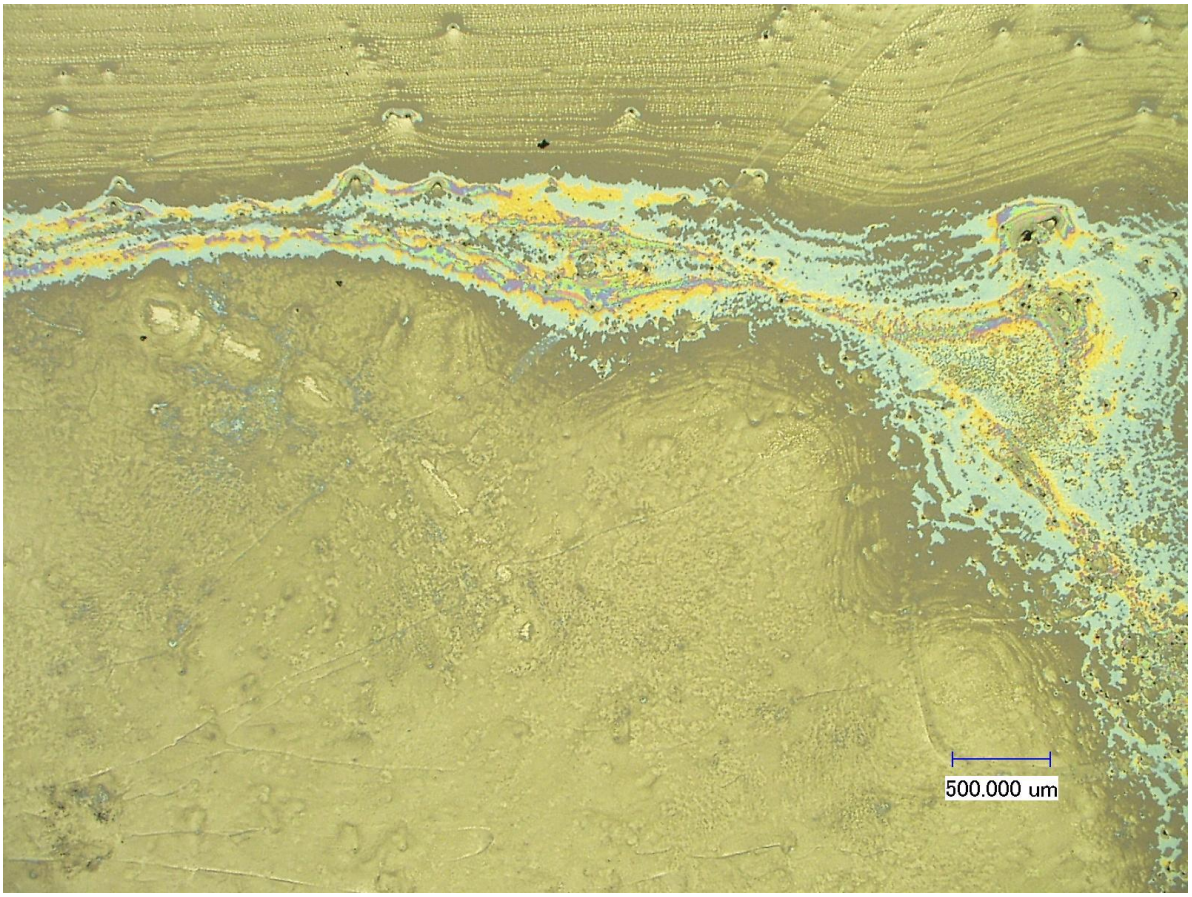

Figure. 18. Spot centre for PSS-EtOH solution (3.13 mg/ml, 0.2 s at 1.5 bar, 8 cm).

On some samples' surfaces dendrite structures were identified (figure 19) after long-distance deposition (8 cm) with a low-concentration solution (< 1.56 mg/ml). This can be explained as a result of a certain hydrophilicity of a substrate – although hydrophilicity is high, the surface is not enough hydrophilic to let the solution easily flow over it. Some microfluidic streams were forming during the deposition as the result of an in-plane gas flow overcoming the local surface tension, thus leading to the formation of dendrite stream structures of monolayer PSS after drying. The inverse dendrite structure (figure 20) was observed after the deposition at 4 cm distance and 3 bar (1.56 mg/ml EtOH-PSS solution). Though its formation is difficult to explain properly, it might be connected with some certain flows that took place at that exact region.

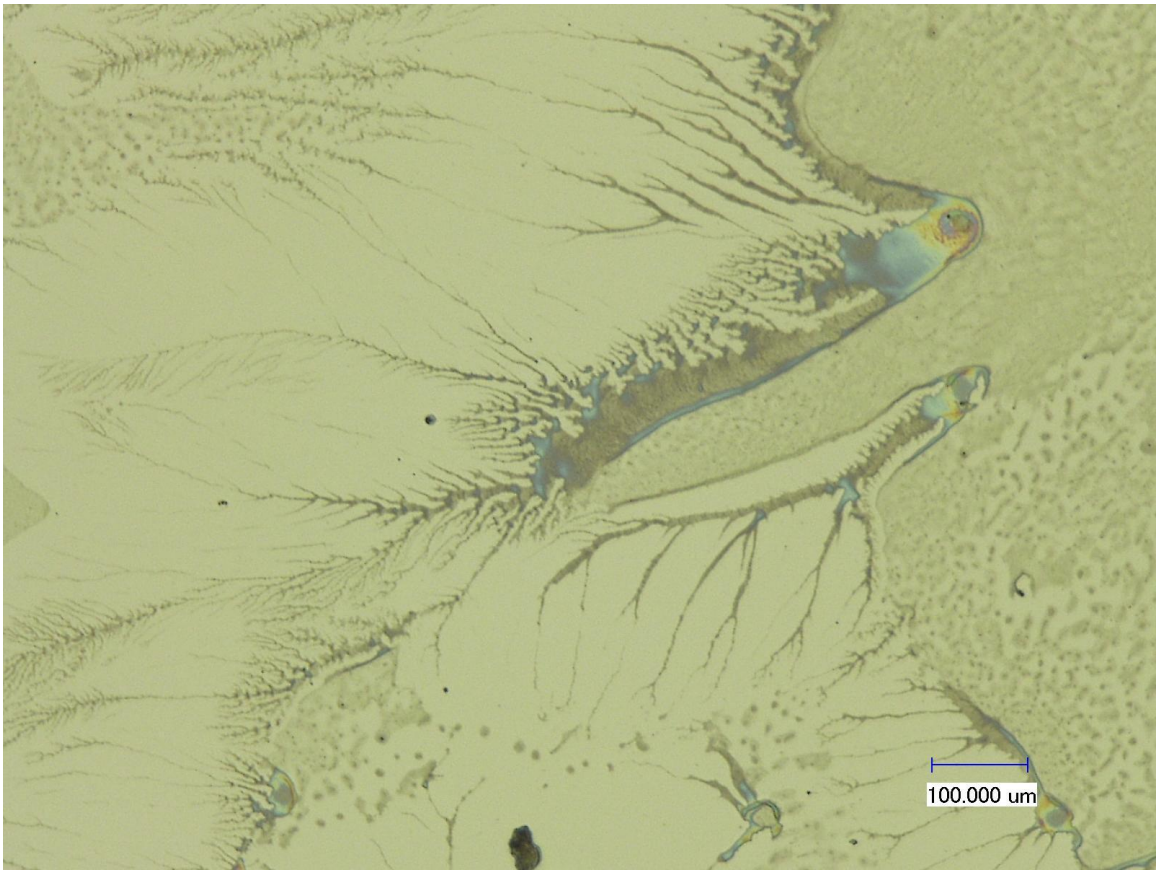

Figure 19. Dendrite stream structures on the sample made at 1.5 bar and 8 cm (0.2 s) from EtOH-PSS solution (0.75 mg/ml).

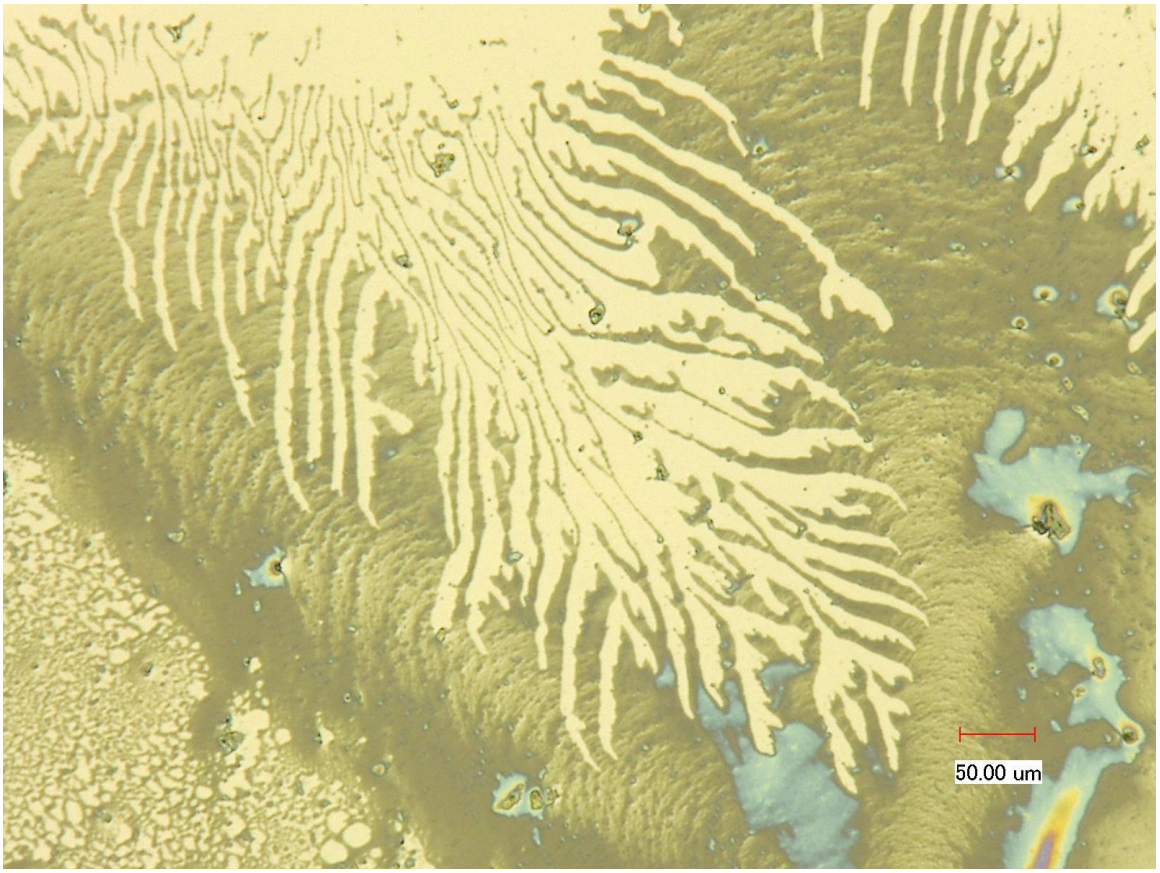

Figure 20. The inverse dendrite structure observed on the sample made at 3 bar and 4 cm distance (0.2 s) from EtOH-PSS solution (1.56 mg/ml).

For $H_2O$-PSS solutions the spot centre is very well seen as was pointed out above. For all solution concentrations the samples obtained during 1 s deposition were very colourful. For short pulses (0.2 s) the samples showed much less colour and a lot of homogeneous brown regions. Strangely enough, we observed flower-like fractals near the edges of substrates for both 0.75 and 1.56 mg/ml concentrations (figure 21). If magnified, the "flowers" look also like dendrites made from microstreams (figure 22).

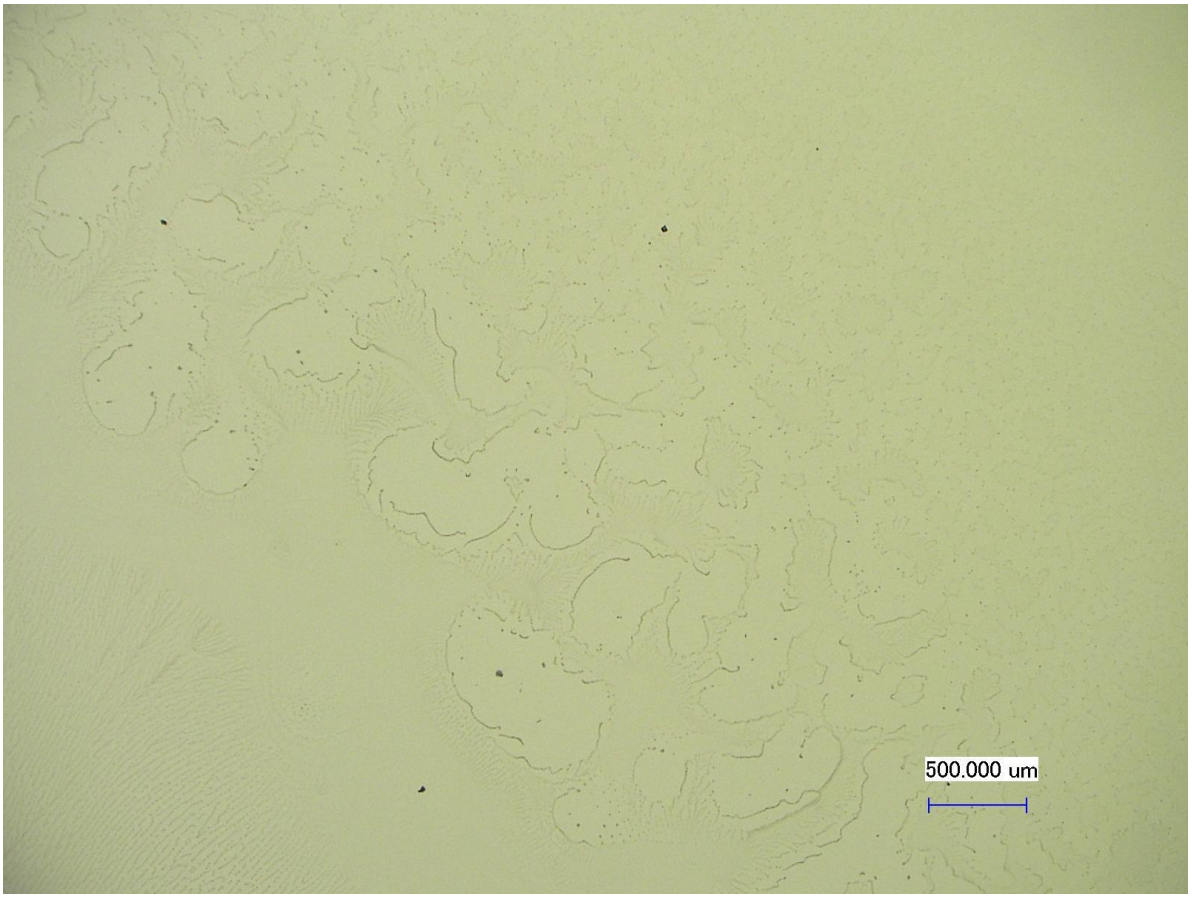


Figure 21. Fractals observed on the edge of the sample made at 3 bar and 8 cm distance (0.2 s) from $H_2O$-PSS solution (1.56 mg/ml).

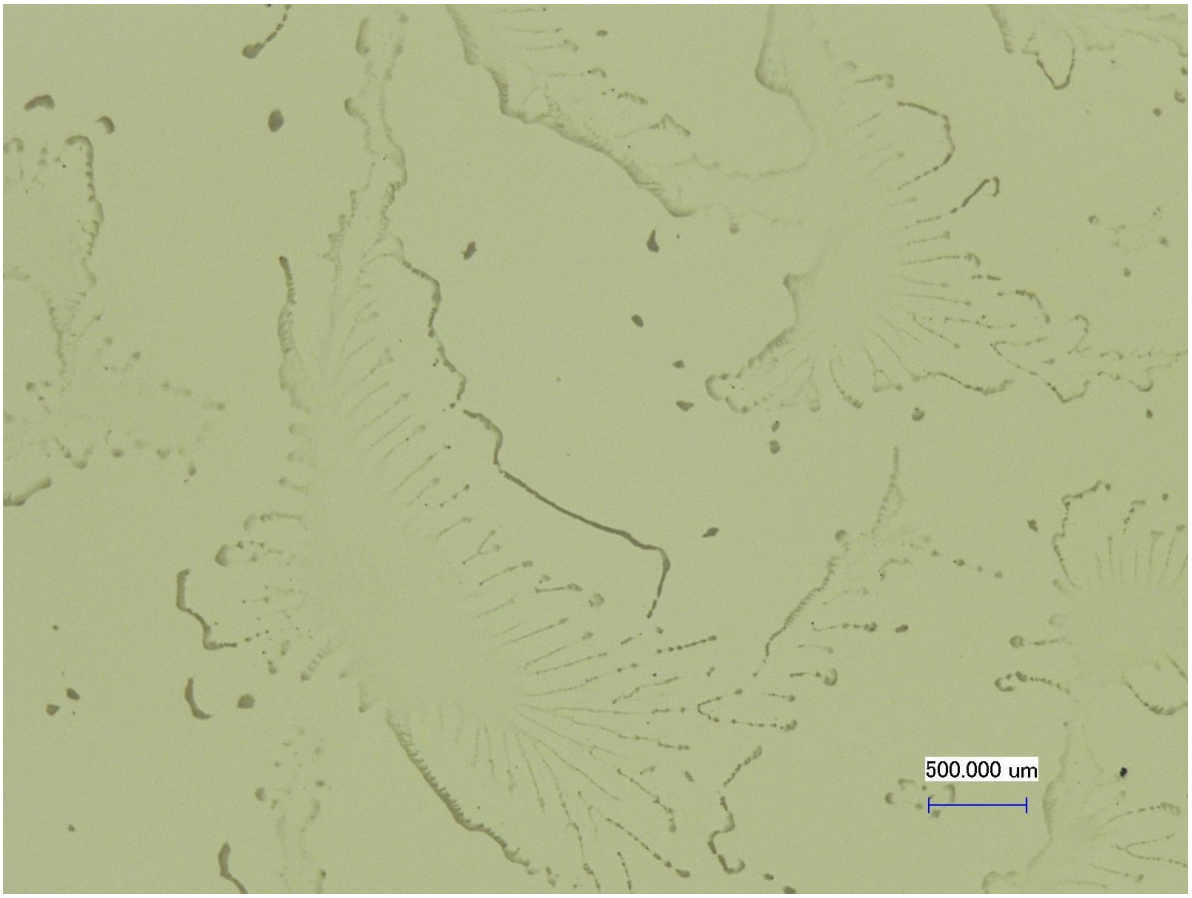

Figure 22. The magnified dendrite-like “flowers” (the sample made at 3 bar and 8 cm distance (0.2 s) from $H_2O$-PSS solution (1.56 mg/ml)).

Another interesting thing that whas been observed is the formation of the stream structure in the presence of turbulences (figure 23). In the left lower edge of figure 23 some surface defect (which is presumably a big random drop of the solution) is seen. During deposition the in-plane flow forced the fluid streams go around this defect, thus producing a beautiful map of stream velocities in 2D.

Figure 23. The in-plane flow making the streams go around the inhomogeneity on a surface, producing a "2D-turbulency"-like picture.

# *GISAXS experiments*

## Introduction

Grazing incidence small angle x-ray scattering (GISAXS) is a common method for studying surfaces and interfaces that combines features of diffuse X-ray Reflectivity and SAXS. It was invented in 1989 by J.R. Levine, J.B. Cohen and Y.W. Chung [18]. Since GISAXS is non-destructive, a non-contact method and it does not require special sample preparation, it is widely used as *in situ* technique to conduct time-resolved investigations of chemical reactions. The GISAXS technique extracts information about possible periodicity in a system and size distribution of units that make periodic structures. The typical GISAXS geometry is shown in figure 24. [23, 24, 25]

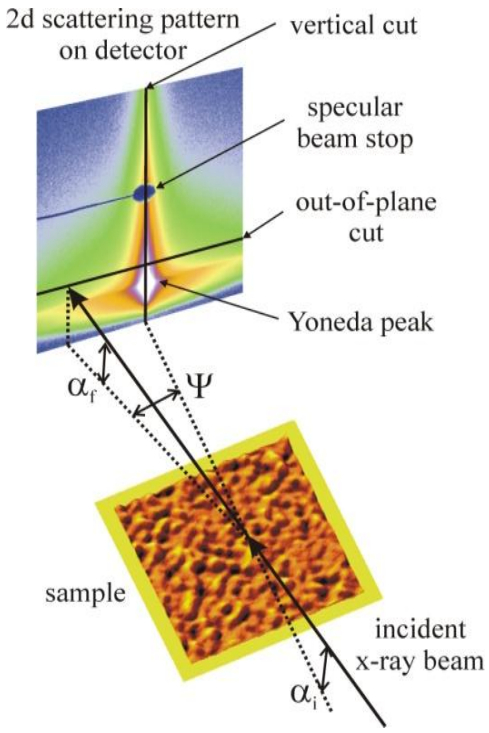

Figure 24. GISAXS geometry. Taken from [25].

These GISAXS measurements at HASYLAB, DESY were made using the DORIS III storage ring's beamline BW4 designed for small and wide-angle X-ray scattering. A schematic layout of the beamline is shown on the figure 25. The general layout of the beamline allows experiments in small-, ultra-small- and wide-angle X-ray scattering in transmission and reflection (grazing-incidence) geometry. At the BW4 beamline characteristic structures from a few micrometers down to a few Angstrom can be resolved.

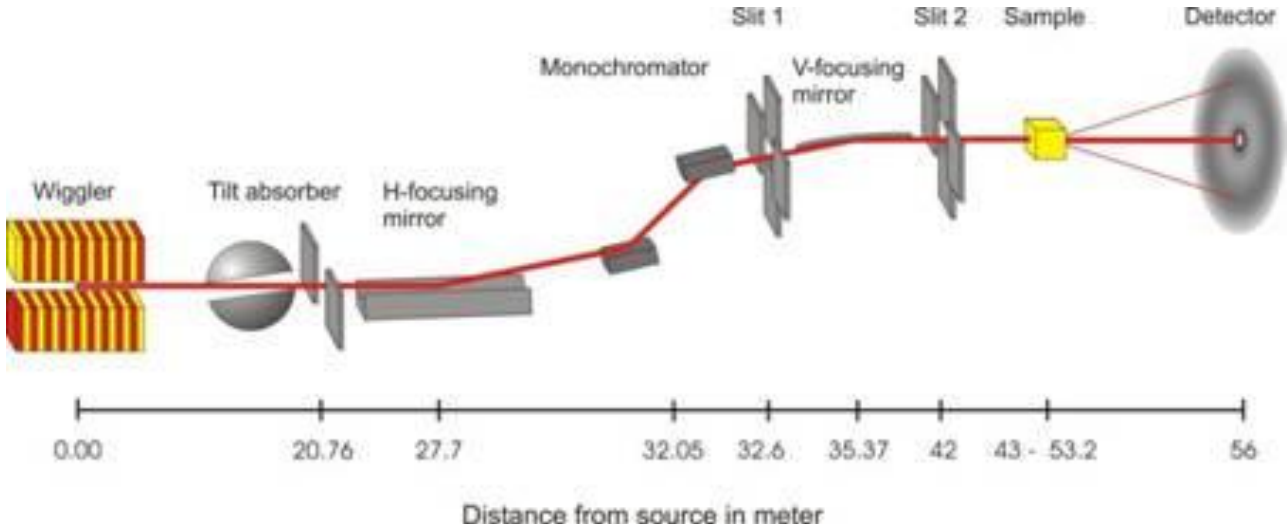

Figure 25. A schematic layout of the beamline. Taken from [16].

# The structure of the BW4 beamline

Since in grazing incidence measurements a small spot size is needed, first a slit system is used to pre-define the beamsize (400 x 400 $\mu m^2$). The moderately micro-focused beam (20 x 40 $\mu m^2$) is achieved by a set of Beryllium compound refractive lenses. The sample stage has 6 degrees of freedom (3 translational and 3 rotational) to accurately position the sample. The position of the sample is shown on the figure 26. To avoid the scattering by air molecules a vacuum is made between the specimen holder and the detector. Two beamstops are needed to prevent the damage of the detector. One for the primary beam and one for the specular beam ($\alpha_i = \alpha_f$). Specular beam corresponds to the directly reflected beam from the sample surface. The direct beam is much stronger than the reflected one. The two-dimensional scattering pattern is captured by a CCD detector. Beam energy can be varied in the range of 4 to 20 keV.

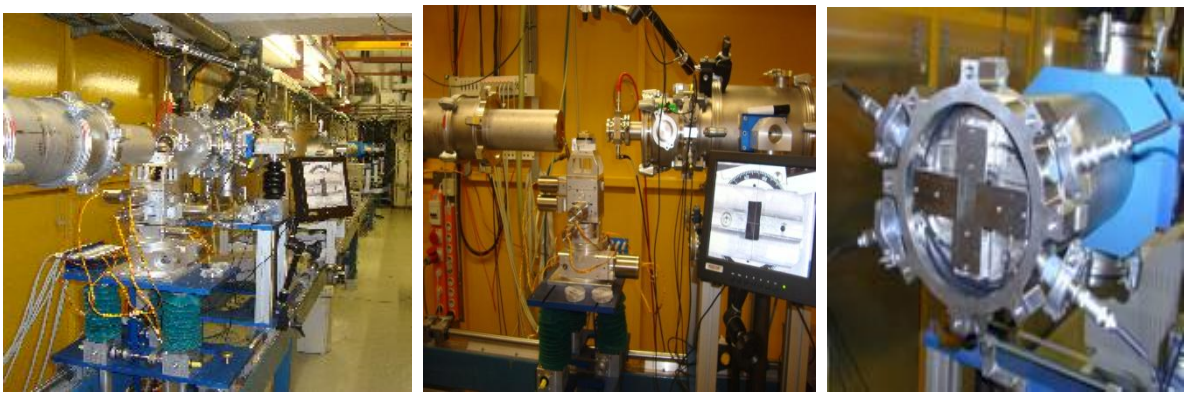

Figure 26. Beamline, specimen stage system and a slit system.

# Measurements

For studying polymer samples using GISAXS a setup was used where the samples were at a distance of 2005 mm away from the detector. The incident angle was larger than the critical angle of the polymers ($\alpha_c$(PS) = 0.138°) sprayed on the sample. Thus, the following parameters were used:

| | |
|---|---|
| Wavelength | 0.138 nm |
| Micro-focused beam size | 23 x 34 $\mu m^2$ (vert. x horiz.) |
| Sample-detector distance ($D_{sd}$) | 2005 mm |
| CCD detector | MARCCD165-detector (2048 x 2048) |
| Incidence angle | $\alpha_i$ = 0.401° |

This setup enables to resolve characteristic structures from approximately 3 to 900 nm.
After positioning the sample the maximum acquisition time was determined in order to avoid saturation of the detector using the following equation:

$$\frac{t_{test}}{I_{\max test}} = \frac{t_{measurement}}{I_{forDettector}},$$

where $I_{\text{for Detector}}$ = 60 000. [22]

# GISAXS data analysis

Fit2D software was used to analyze the scattering patterns [17]. The components of the scattering vector **q** are defined as follows [24]:

$q_x = 2\pi(\cos\psi\ \cos\alpha_f - \cos\alpha_i)/\lambda$,

$q_y = 2\pi(\sin\psi\ \cos\alpha_f)/\lambda$,

$q_z = 2\pi(\sin\alpha_i+\sin\alpha_f)/\lambda$,

where $\lambda$ is the wavelength, $\alpha_i$ is the incident angle, $\alpha_f$ is the vertical scattering angle Langmuir-Blodgett was also used to prepare samples. In Langmuir-Blodgett method amphiphilic molecules are first deposited on the surface. When reducing the area the surface pressure increases and a phase transition from gas to liquid occur. Surfactant molecules pack very closely in to a solid state, the forming monolayer reduces the surface tension. A schematic layout of the Langmuir-Blodgett method is shown in scheme 1.
and $\psi$ is the out-of-plane scattering angle.

The vertical slices are called *detector scans* and are performed at $q_y$=0 (*off-detector scans* for $q_y \neq 0$). Horizontal slices are named *out-of-plane scans* and are performed for constant values of $q_z$. By the equation $d=2\pi/q$ the corresponding characteristic length *d* of the sample in real space can be calculated from the scattering pattern.

The so called Yoneda peak or characteristic structure peak (figure 24, 27) appeared around pixel Y = 1002 in vertical direction corresponding to the critical angle of PS. At this position, the out-of-plane cut has been performed. This one and the vertical scan at pixel X = 1035 were selected for studying the structure of the polystyrene thin film.
The out-of-plane angle Ψ can be calculated using the following equation:

$$\psi = \tan^{-1}\frac{pixeldis\tan ce \times pixelsize}{D_{sd}},$$

where $D_{st}$ is the distance between the symmetry center and a pixel position, and $D_{SD}$ is the distance between a sample and the detector.

The XGenplot software was used to plot the intensity patterns. The structural information can be investigated in horizontal region in Yoneada peak area. The plots of the logarithm of intensity vs. vector component $q_y$ were made in order to obtain characteristic structural information of the thin film and surface structures.

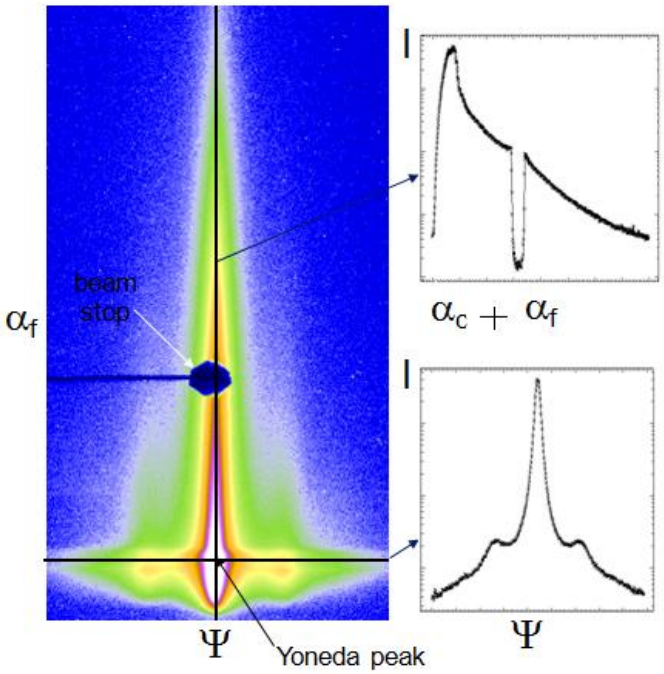


Figure 27. Typical GISAXS pattern of ordered nanostructures in thin film with the characteristic Yoneda peak. The corresponding vertical and horizontal scans are shown on the right hand side.

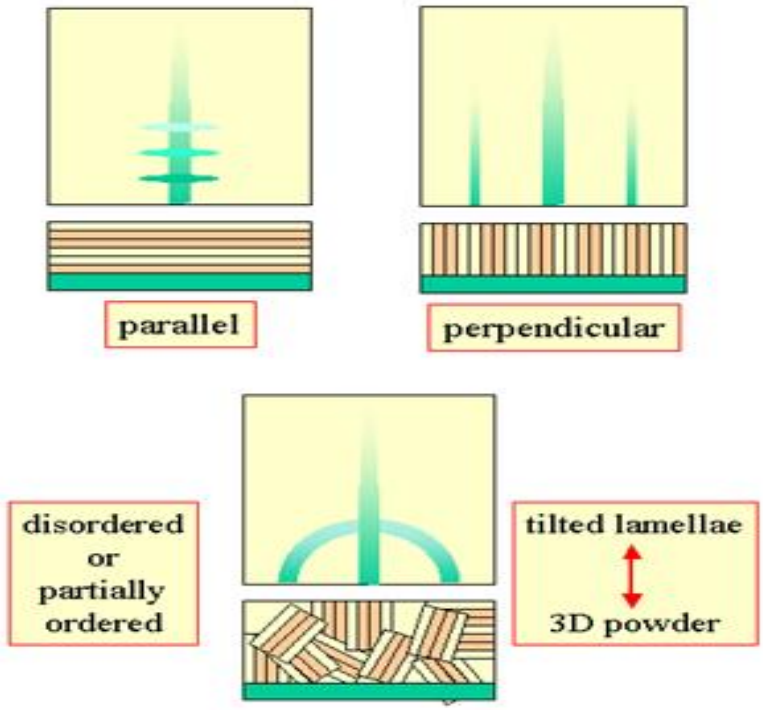


*Figure.28 GISAXS measurements provide information of parallel, perpendicular or partially or disordered structures. Taken from [21].*

For some first qualitative judgment of some GISAXS scattering patterns figure 28 shows the influence of some basic thin film characteristics on the intensity distribution in the potential scattering pattern. In general, domains or sub-layers in the thin film can be arranged parallel, perpendicular and disordered or partially ordered

# Discussion of GISAXS results

Three samples were chosen to be characterized by GISAXS. The properties of the samples are listed in table 1. Every sample was measured twice, in the spot centre as well as of the outer region of the spot in order to study the rim structures. The 2D patterns of the measured samples are presented in figure 28-30 in a logarithmic scale.

*Table.1 Properties of the measured samples*

| **Name of the sample** | **Solution** | **Spraying time (s)** | **Pressure (bar)** | **Distance (cm)** | **Concentration µmg/L** |
|---|---|---|---|---|---|
| C8 | PSE | 0.2 ± 0.1 | 3 ± 0.1 | 4 ± 0.1 | 3.125 |
| C7 | PSE | 0.2 ± 0.1 | 3 ± 0.1 | 4 ± 0.1 | 6.250 |
| C3 | PSE | 0.2 ± 0.1 | 3 ± 0.1 | 8 ± 0.1 | 3.125 |

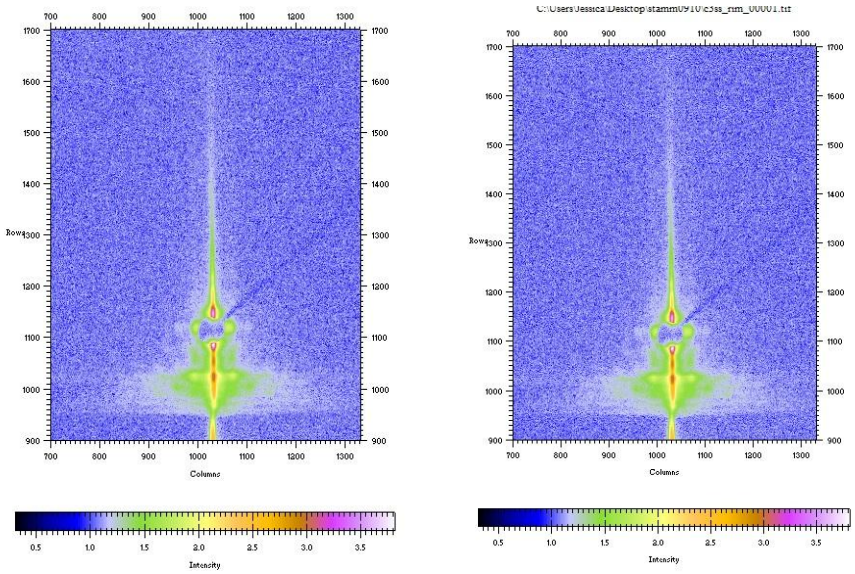


Figure 29. The patterns of the spot centre and the rim structure of the sample C3.

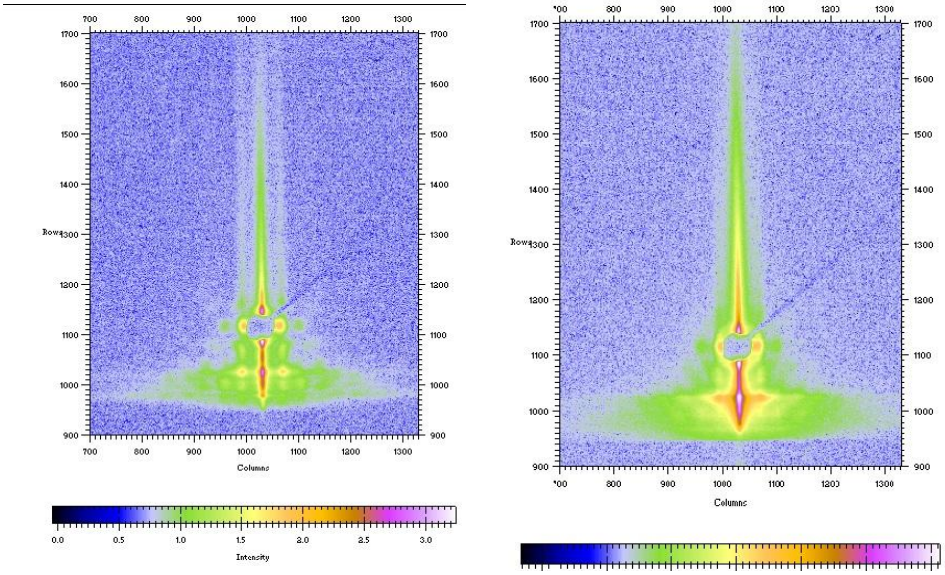


Figure 30. The patterns of the spot centre and the rim structure of the sample C7.

.

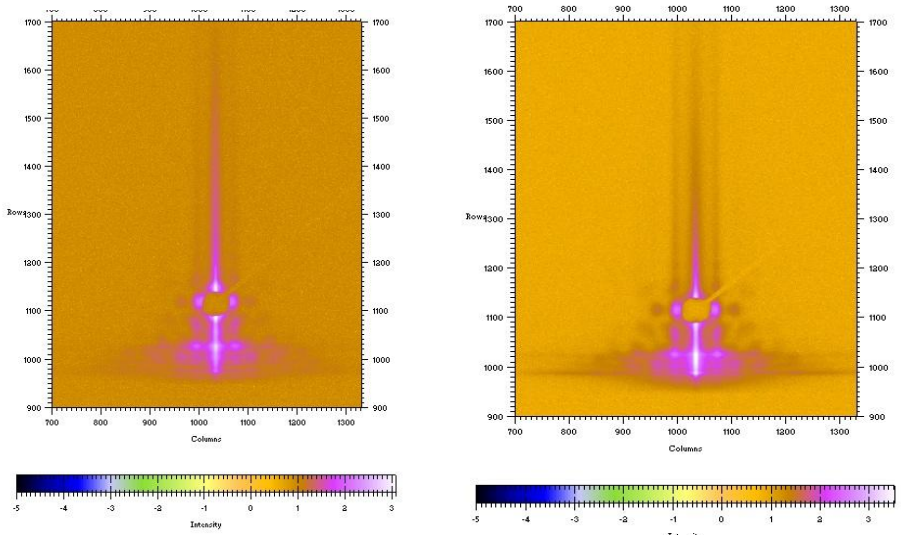


Figure 31. The patterns of the spot centre and the rim structure of the sample C8.

Judging by the patterns, PS spheres are arranged mostly hexagonal order. For those samples with colorful rims and light-brown centre the intensity of hexagonal peaks is higher, consequently indicating the possible multilayer structure of the film in that area. To fully exclude the cubic packing of PS spheres or at least to find any evidence of polymer packing further investigation is needed.

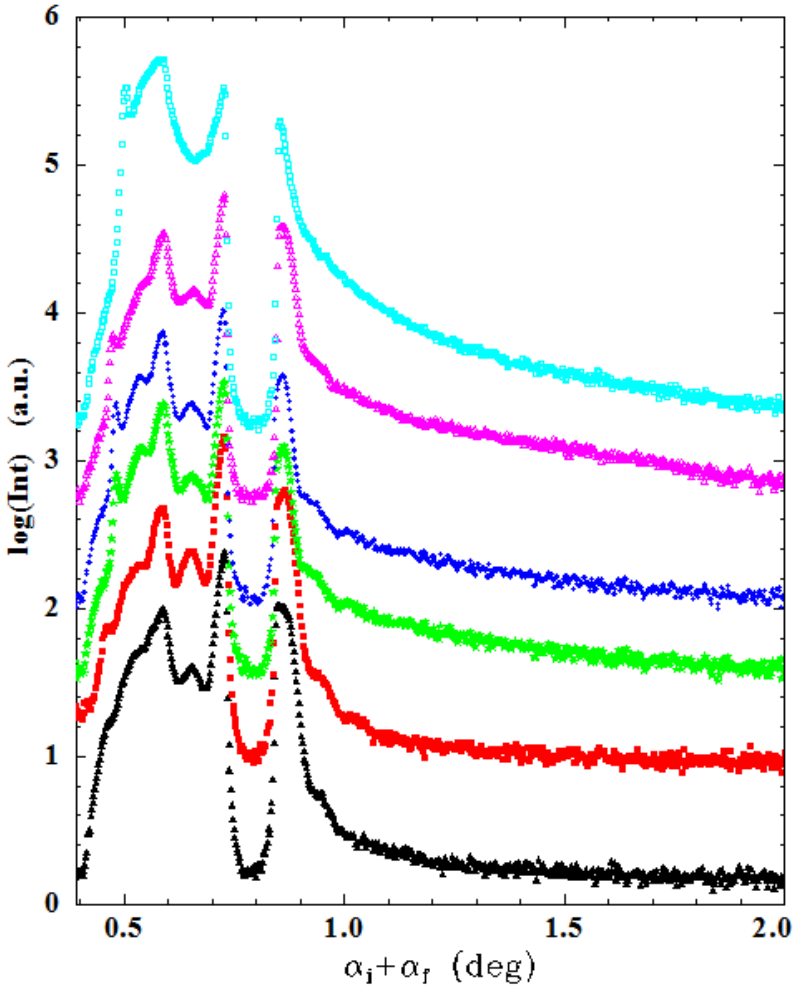


*Figure.30 Compiled vertical cuts of the scattering patterns. In black and red for sample C3 the inner structure and rim structure, green corresponds the inner structure of sample C7 and blue color the rim structure of sample C7. The inner structure of sample C8 is presented in pink and rim-structure in turquoise color.*

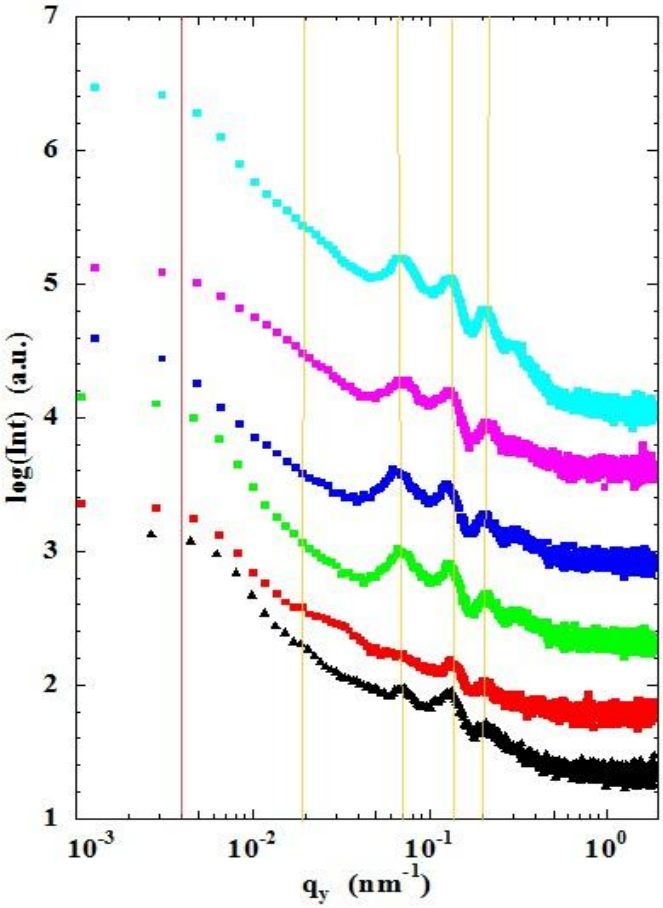


*Figure. 31 Compiled horizontal cuts of the scattering patterns. In black and red for sample C3 the inner structure and rim structure, green corresponds the inner structure of sample C7 and blue color the rim structure of sample C7. The inner structure of sample C8 is presented in pink and rim-structure in turquoise color. The solid red line represents the resolution limit of the experimental setup corresponding to the largest resolvable characteristic length scale $d_{max}$ = 900 nm.*

Several characteristic lengths can be obtained from the horizontal cuts as depicted in figure 31. AFM-measurements are needed to assign this structures but the droplet sizes can be approximated to vary between 90-20nm.

*Table.2 Characteristic lengths of the sprayed samples*

| C3 inner [nm] | C3 rim structures [nm] | C7 inner [nm] | C7 rim structures [nm] | C8 inner [nm] | C8 rim structures [nm] |
|---|---|---|---|---|---|
| 90nm | - | 90 | 90 | 0.90 | 90 nm |
| 49 nm | - | 49 | 49 | 49 | 49 |
| 32 | 32 | 32 | 32 | 32 | 32 |
| 22 | 22 | 22 | 22 | 22 | 22 |

# Conclusions

GISAXS is suitable for studying internal structures in thin films and structures on surfaces, e.g. cellulose thin films and (mono) layers of polystyrene solution of ethanol and water. While GISAXS is an independent experimental technique, complementary measurements are necessary, e.g. optical microscopy, atomic force microscopy and scanning electron microscopy to assign specific morphological characteristics to the obtained characteristic length scales of the sprayed PS-spheres in thin film. The study of samples will continue by making AFM measurements.

In summary, we have shown that a variety of different spot patterns can obtained by spray deposition. The spot structure was demonstrated to dramatically vary depending on the nozzle-substrate distance, the pulse time, the in-nozzle pressure, substrate and solvent nature. A thorough consideration of the influence of conditions on the spot structure has been given in this report. The water- and ethanol-ink solutions produced absolutely different spot patterns. The ethanol-made spots were continuous; their shapes were ‘arm’-like at short deposition distances, then gradually became perfect discs near the transition distance, and finally they started to be made of randomly distributed droplets. On the contrary, at short distances the water-made spots consisted of small droplets in the middle and large drops in the outer region. At approaching the transition distance drops became of a similar size, but after that the inner region consisted of large drops, while the surrounding region was made of very small droplets. A significant deposition of mist on the substrate was observed at large deposition distances which indicated the presence of strong turbulence in the jet as well as a high velocity in the in-plane flow on the substrate. It was shown that to deposit a smooth and continuous film one is required to perform the deposition near the transition distance (the exact position of a substrate depends on a setup used). We have demonstrated that a higher pressure changes the cone structure in way that can be considered as a nozzle shift to larger distances, thus producing a better-quality spot compared to low-pressure deposition at the same distance. In this manner one can imagine that the increase in pressure makes similar effect on the spot structure as the shift of the target closer to the spray source.

# Acknowledgments

We would like express special thanks to Matthias Schwartzkopf, Dr. Jan Perlich and Dr. Stpehan V. Rooth for the supervision, valuable discussions and taking care of us. Thanks to Dr. Ulla Vainio for showing facilities at HASYLAB and many kindly helps. We would also like express thanks to our group, especially to Dr. Adeline Buffet and Dr. Mottakin Abul Kashem. Our sincere acknowledgements to Prof. Joachim Meyer, Dr. Rainer Gehrke, Andrea Schrader, and other people involved in the summer student program. Thanks also to professor Ritva Serimaa for her support to participate in the Desy summerstudent program. It was a great pleasure to be here.

# References

[1] K. L. Choy. *Chemical vapour deposition of coatings*. Prog. in Mater. Sci. Vol. **48**, Issue 2 (2003), pp. 57-170.

[2] Gorbenko OY, Samoilenkov SV, Graboy IE, *et al. Epitaxial stabilization of oxides in thin films*. Chem. of Mater. Vol. **14**, Issue 10 (2002), pp. 4026-4043.

[3] Paolo Politi *et al. Instabilities in crystal growth by atomic or molecular beams.* Phys. Rep. **324**, Issues 5-6 (2000), pp 271-404.

[4] A.A. Voevodin, M.S. Donley. *Preparation of amorphous diamond-like carbon by pulsed laser deposition: a critical review.* Surface and Coatings Tech. **82** (1996), pp. 199-213.

[5] Niesen TP, De Guire MR. Review: *Deposition of ceramic thin films at low temperatures from aqueous solutions*. J. of Electroceramics. V. **6**, Issue 3 (2001), pp. 169-207.

[6] Brian W. Gregory and John L. Stickney. *Electrochemical atomic layer epitaxy (ECALE)***.** J. of Electroanalytical Chemistry, Vol. 300, Issues 1-2 (1991), pp. 543-561.

[7] Jiang P, McFarland MJ. Large-scale fabrication of wafer-size colloidal crystals, macroporous polymers and nanocomposites by spin-coating. J. Am. Chem. Soc. V. 126, Issue 42 (2004), pp. 13778-13786.

[8] Stephen R. Forrest. The path to ubiquitos and low-cost organic electronic appliances on plastic. Nature 428, 911-918 (29 April 2004)

[9] Marta Kolasinska, Rumen Krastev, Thomas Gutberlet, and Piotr Warszynski. *Layer-by-Layer Deposition of Polyelectrolytes. Dipping versus Spraying.* Langmuir, **25**, 1224-1232 (2009).

[10] Mariya Aleksandrova. *Spray Deposition of Multilayer Polymer Structures for Optoelectronic Applications*. e-J. Surf. Sci. Nanotech. Vol. 7 (2009) 859-862.

[11] Douglas L. Schulz,* Martin Pehnt, Doug H. Rose, Ed Urgiles, Andrew F. Cahill, David W. Niles, Kim M. Jones, Randy J. Ellingson, Calvin J. Curtis, and David S. Ginley. *CdTe Thin Films from Nanoparticle Precursors by Spray Deposition.* Chem. Mater., 1997, 9 (4), pp 889–900.

[12] Xin Zhao, Claire Hinchliffe, Colin Johnston, Peter J. Dobson, Patrick S. Grant. *Spray deposition of polymer nanocomposite films for dielectric applications.* Materials Science and Engineering B **151** (2008) 140–145.

[13] Doojin Vak, Seok-Soon Kim, Jang Jo, Seung-Hwan Oh, Seok-In Na, Juhwan Kim, and Dong-Yu Kim. *Fabrication of organic bulk heterojunction solar cells by a spray deposition method for low-cost power generation*. APL **91**, 081102 (2007).

[14] R. Green, A. Morfa, A. J. Ferguson, N. Kopidakis, G. Rumbles, S. E. Shaheen. *Performance of bulk heterojunction photovoltaic devices prepared by airbrush spray deposition.* APL **92**, 033301 (2008).

[15] Shreen Eletribi. *Dispersion of Water Sprays in a Transverse Air Jet and the Aging Spray Nozzle.* Massachauts Institute of technology February (1999).

[16] http://hasylab.desy.de/facilities/doris_iii/beamlines/bw4/experimental_station/detectors/index_eng.html visited 8.9.2010

[17] http://www.esrf.eu/computing/scientific/FIT2D/ visited 30.8.2010

[18] J.R. Levine, J.B. Cohen and Y.W. Chung.P. Georgopoulos *Grazing-incidence small-angle X-ray scattering: new tool for studying thin film growth.* J. Appl. Crystallogr. 22 (1989) 528-532.

[19] BW4 Beamline Manual Version 0.8.2 from Novemner 2008 –some guidence for measuring

[20] P.Muller-Burschbaum *Structure Determination in Thin Films Geometry using Grazing Incidense Small-Angle Scatttering* Polymer surface and interfaces 2008, 17-46

[21] -nice GISAXS tutorial

[22] BW4 Beamline Manual Version 0.8.2 from Novemner 2008 – some guidance for measuring

[23] P. Müller-Buschbaum *Grazing incidence small-angle X-ray scattering:an advanced scattering technique for the investigationof nanostructured polymer films.* Anal Bioanal Chem 376 : 3–10 DOI 10.1007/s00216-003-1869-2 (2003)

[24] P.Muller-Burschbaum *Structure Determination in Thin Films Geometry using Grazing Incidense Small-Angle Scatttering* Polymer surface and interfaces, 17-46 (2008)

[25] J. Perlich, L. Schulz, M. M. Abul Kashem, Y.-J. Cheng, M. Memesa, J. S. Gutmann, S. V. Roth and P. Müller-Buschbaum *Modification of the Morphology of P(S-b-EO) Templated Thin $TiO_2$ Films by Swelling with PS Homopolymer* Langmuir, 23, 10299-10306 (2007)

[26] http://www-lfp.cea.fr/ast_visu.php?num=430&lang=ang last visited.8.9.2010